THE XMM-LSS CLUSTER SAMPLE AND ITS COSMOLOGICAL APPLICATIONS

M. Pierre, F. Pacaud[1] and the XMM-LSS consortium[2]

[1]DAPNIA/SAp CEA Saclay, 91191 Gif sur Yvette, France
[2] http://vela.astro.ulg.ac.be/themes/spatial/xmm/LSS/cons_e.htmle

ABSTRACT

We present the X-ray source detection procedure that we have developed for the purpose of assembling and characterizing controlled samples of cluster of galaxies for the XMM Large Scale Structure Survey. We describe how we model the selection function by means of simulations: this leads us to define source classes rather than flux limited samples. Focussing on the CFHTLS D1 area, our compilation suggests a cluster density higher than previously determined from the deep ROSAT surveys above a flux of 2×10^{-14} erg cm^{-2}s^{-1}. We also present the L-T relation for the 9 brightest objects in the area. The slope is in good agreement with the local correlation. The relation shows luminosity enhancement for some of the $0.15 < z < 0.35$ objects having $1 < T < 2$ keV, a population that the XMM-LSS is for the first time systematically unveiling.

Key words: Surveys, X-ray analysis, clusters of galaxies.

1. INTRODUCTION

The question of cosmic structure formation is substantially more complicated than the study of the spherical collapse of a pure dark matter perturbation in an expanding Universe. While it is theoretically possible to predict how the shape of the inflationary fluctuation spectrum evolves until recombination, we hardly understand the subsequent galaxy, AGN and cluster formation because of the problems of non-linear growth and the feedback from star formation. Consequently we cannot use the statistics of visible matter fluctuations to constrain the nature of the Dark Matter and Dark Energy without developing this understanding of non-gravitational processes.
Clusters, the most massive entities of the Universe, are a crucial link in the chain of understanding. They lie at the nodes of the cosmic network, and have virialized cores, but are still growing by accretion along filaments. The rate at which clusters form, and the evolution of their space distribution, depends strongly on the shape and normalization of the initial power spectrum, as well as on the Dark Energy equation of state (e.g. Rapetti et al. (2005)). Consequently, both a 3D mapping of the cluster distribution and an evolutionary model relating cluster observables to cluster masses and shapes (predicted by theory for the average cluster population) are needed to test the consistency of the "CMB WMAP concordance cosmology" with the properties of clusters in the low-z Universe. With its mosaic of 10 ks overlapping XMM pointings, the XMM Large Scale Structure survey (XMM-LSS) has been designed to detect a significant fraction of the galaxy cluster population out to a redshift of unity over an area of several tens of square degrees, so as to constitute a sample suitable to address the questions outlined above (Pierre et al. 2004). The trade-off in the survey design was depth versus coverage, keeping within reasonable total observing times.
This configuration allows investigation of the cluster population down to a depth of about 10^{-14} erg cm^{-2}s^{-1} which is comparable to the deepest ROSAT serendipitous surveys (Rosati et al. 2002). However, observations are performed with a narrower PSF (FWHM $\sim$ 6" for XMM vs $\sim$ 20 " for the ROSAT PSPC) and very different different instrumental characteristics such as background noise and focal plane configuration. This led us to develop a new X-ray pipeline which is presented in the next section, along with the principles of the computation of the survey selection function. Spectroscopically identified clusters undergo detailed measurements, which enabled us to track the evolution of the low-mass end of the cluster population (Sec. 3). Source statistics and the L-T relation for the CFHTLS D1 area are presented in Sec. 4. In the following, we assume a ΛCDM cosmology and give all fluxes in the [0.5-2] keV band.

2. XAMIN – A NEW X-RAY PIPELINE

2.1. Design

The two major requirements of the XMM-LSS X-ray processing were to reach the sensitivity limit of the data in a statistically tractable manner in terms of cluster detection efficiency, and hence to calculate the selection function

of the detected objects. The package that we have developed, `Xamin`, combines the sensitivity of the multi-resolution wavelet analysis for source detection with the rigour of a likelihood analysis for assessing the significance of the detected sources, handling the complex XMM instrumental characteristics. Both steps use Poisson statistics. The whole procedure has been validated by means of extensive simulations of point-like and extended sources (Pacaud et al. 2005).

2.2. Source classification

Simulations of the LogN-LogS X-ray point source population give for `Xamin` a 90% completeness level down to a flux of 4×10^{-15} erg cm^{-2}s^{-1} for 10 ks exposures. As a rule of thumb, the corresponding sensitivity for 'typical' cluster sources is 2-3 times higher. However, cluster detection efficiency depends not only on the object flux and size, and the instrumental PSF, but also very much on the background level and on the detector topology such as CCD gaps and vignetting, as well on the ability of the pipeline to separate close pairs of pointlike sources. We thus stress that the concept of sky coverage, i.e. the fraction of the survey area covered at a given flux limit, is strictly valid only for point-sources because, for faint extended objects, the detection efficiency is surface brightness limited (rather than flux limited). Moreover, since the faint end of the cluster luminosity function is poorly characterised at $z > 0$, it is not possible to estimate a posteriori what fraction of groups remain undetected, unless a cosmological model is assumed, along with a thorough modelling of the cluster population out to high redshift.

Consequently, with the goal of constructing deep controlled samples suitable for cosmology we define, rather than flux limits, two classes of extended sources corresponding to specific levels of contamination and completeness. The selection is performed in the `Xamin` output parameter space defined by `extent likelihood, extent, detection likelihood`. Selection criteria have been established by means of extensive simulations for cluster apparent core-radii (extent) ranging from 10" to 100", and total number counts from 50 to 1000. The cluster surface brightness distribution was assumed to follow a β-model, with $\beta = 2/3$. The C1 class is defined to have "no contamination". i.e. no point sources missclassified as extended. For the C2 class, selection criteria are relaxed such as to allow for 50% contamination by spurious extended sources. The classification has been in turned checked against some 60 spectroscopically XMM-LSS clusters confirmed to date. C1 clusters are high surface brightness extended objects; this selection inevitably retains a few nearby galaxies, but these are readily discarded from the sample by inspection of optical overlays. The C2 sample includes fainter clusters than C1, and also a number of nearby galaxies, saturated point sources and unresolved pairs, as well as cases badly effected by CCD gaps; the contamination is a posteriori removed by the visual inspection of the optical overlays as well as by the outcome of the spectroscopic identification programme. The principle of the procedure is illustrated in Fig. 1.

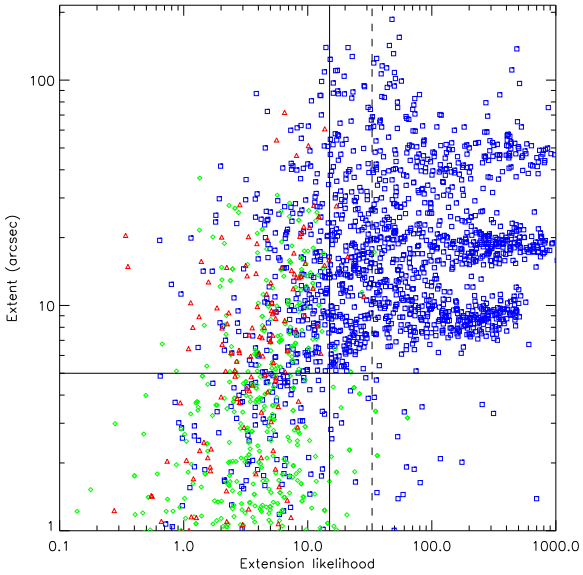

Figure 1. Cluster selection criteria in the `Xamin` *parameter space populated by simulations. Point sources are represented by green diamonds, clusters by blue squares; red triangles indicate spurious sources. The horizontal and vertical solid lines delineate the C1+C2 class. The dotted vertical line indicates the restriction to the C1 class to which the* `detection likelihood` > 32 *condition was added, guaranteing an uncontaminated sub-sample of clusters*

2.3. The survey selection function

In parallel, simulations provide the necessary basis for the computation of the selection function. They allow us to derive detection probabilities as a function of source core-radius and countrate for any exposure time, background level and position on the detector (Fig. 2). As an example, we show the dn/dz prediction for the C1 cluster population, assuming the following model: ΛCDM cosmology (Bennett et al. 2003) + P(k) power spectrum with transfer function from Bardeen et al. (1986) and comoving halo number density from the Sheth & Tormen (1999) mass function, $M_{200} - T$ relation from Arnaud et al. (2005), $L-T$ relation from Arnaud & Evrard (1999) and a constant core radius of 180 kpc. The cluster/group population was simulated down to T = 1 keV (no evolution of the cluster M-T-L scaling laws was assumed, as it is currently unconstrained by observations for the $1 < T < 3$ keV range which constitute the bulk of our population). The predicted C1 dn/dz is shown in Fig. 3, along with the observed redshift distribution of the observed C1 population. The agreement is very satisfactory and the data suggest a deficit of clusters around a redshift of 0.5, probably induced by a cosmic void. Ob-

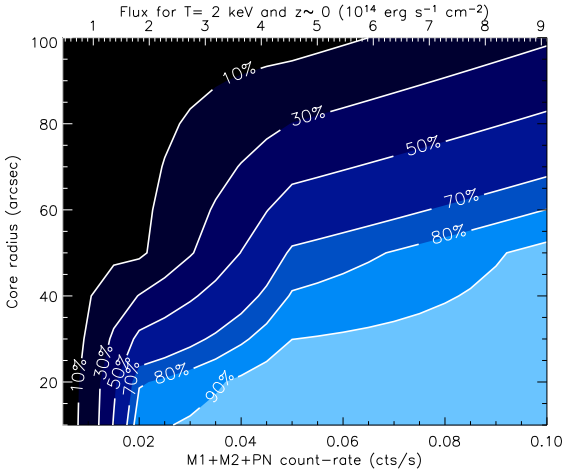

Figure 2. Detection probability for C1-type clusters as a function of count rate and core-radius, averaged for the 20 inner arcmin of the XMM field, and for an exposure time of 10 ks

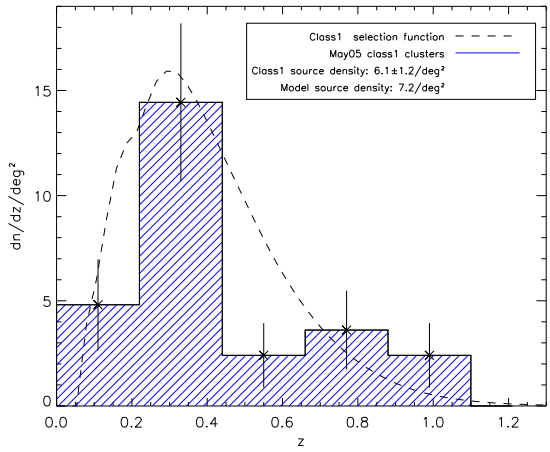

Figure 3. Redshift distribution of the C1 clusters for the current XMM-LSS area: 48 pointings covering 4.6 effective deg^2 *(only the inner 20 arcmin are considered) – that is 29 objects. The dotted line corresponds to the predictions from a simple halo model in a* Λ*CDM cosmology (see text).*

served cluster numbers from the currently available 51 XMM-LSS pointings are $7/\mathrm{deg}^2$ and $12/\mathrm{deg}^2$ for the C1 and C2 class respectively. Finally, we have investigated for our simple cosmological model, to what extent the C1 and C2 classes are comparable to flux limited samples (Fig. 4). The main result is that the C1 sample approaches, in terms of number density, a flux limited sample of about $2\times10^{-14}\ \mathrm{erg\,cm^{-2}s^{-1}}$. But (1) more high-z objects are detected, while nearby low-surface brightness groups are not retained, and (2) the C1 sample is strictly defined from X-ray criteria (and hence is not contaminated) while it would be necessary to examine a large number of sources to clean a putative flux limited sample at $2\times10^{-14}\ \mathrm{erg\,cm^{-2}s^{-1}}$, with many of them not being unambiguously characterized as extended or point-like.

3. CLUSTER MEASUREMENTS

Each spectroscopically confirmed cluster undergoes detailed spectral and spatial fits in order to determine its temperature, flux and bolometric luminosity within R_{500} (standard overdensity radius). In particular, we have demonstrated that, under specific statistical model and binning conditions, we reach a 20% accuracy in temperature measurements with ~ 100 and ~ 300 photons for 1 and 2 keV groups respectively (Willis et al. 2005). It turns out that the C1 cluster sample is almost identical to the sample for which we can measure temperatures.

4. RESULTS FROM THE D1 CFHTLS AREA

The D1 CFHTLS area covers $1\mathrm{deg}^2$ and constitutes the central part of the XMM-LSS (see Pierre et al. (2004) for a general layout of multi-wavelength coverage associated

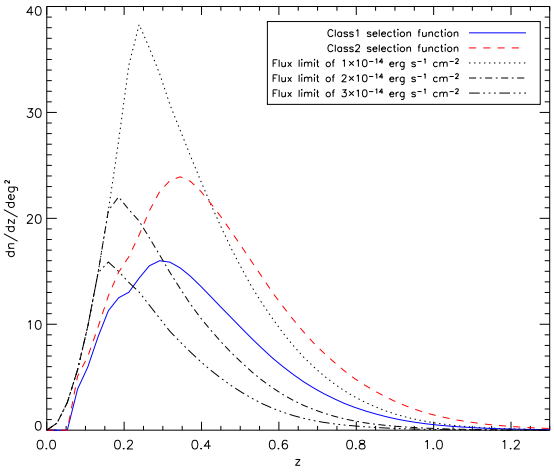

Figure 4. Comparison of the C1 and C1+C2 redshift distribution with various flux-limited samples, assuming the simple cosmological model described in the text

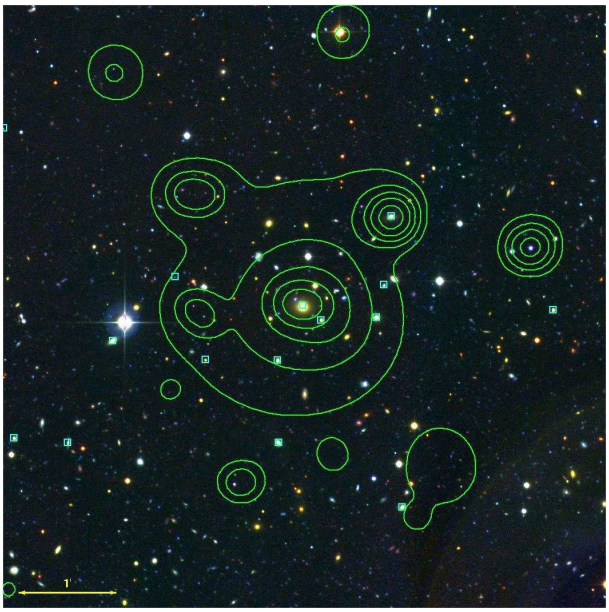

Figure 5. Example of a C1 cluster at z = 0.26 ($F \sim 8 \times 10^{-14}$ erg cm^{-2}s^{-1}). The cluster X-ray contours are overlaid on a u,r,z CFHTLS composite. They are drawn from the co-added [0.5-2] keV MOS1+MOS2+pn mosaic, filtered in the wavelet space using a significance threshold of 10^{-3} for Poisson statistics (not corrected for vignetting). The intensity scale is logarithmic (counts/pixel/second, not corrected for vignetting). Boxes indicate cluster members for which we obtained a redshift using LDSS at the Magellan telescope.

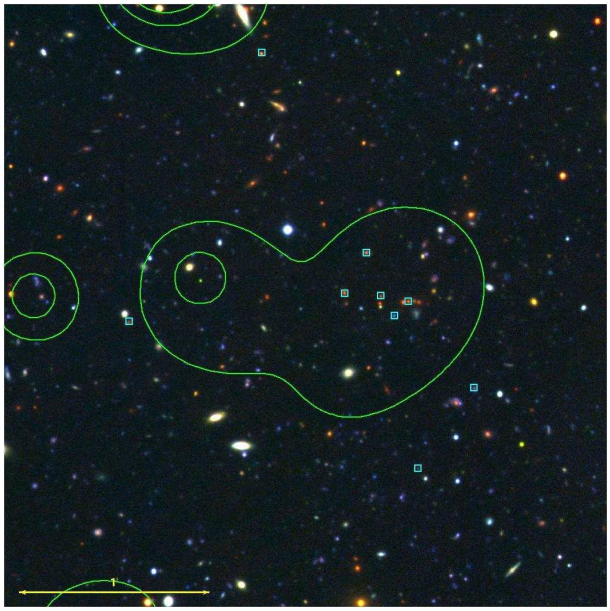

Figure 6. Example of a faint cluster at z = 0.92 at the detection limit ($F \sim 3 \times 10^{-15}$ erg cm^{-2}s^{-1}). The source was not spectroscopically followed-up. Redshift confirmation comes from the VVDS data alone. Same symbols and contours as in Fig. 5

with the XMM-LSS). It includes among others the Vimos VLT Deep Survey (VVDS, Bondi et al. (2003)). We present a summary of the properties of the cluster sample for this region[1]. We have spectroscopically identified 13 clusters over the 0.8 deg^2 effective area. Out of these, 8 are C1 clusters, 1 is classified as C2, and 4 are clusters not entering the classification (very faint objects or clusters contaminated by a point source). The selection function for these 4 latter systems is unknown, but they are interesting objects indicative of our ultimate detection limit, i.e. $\sim 3-5 \times 10^{-15}$ erg cm^{-2}s^{-1}. Two examples are illustrated on Figs. 5 and 6. The C1+C2 clusters span the $0.05 < z < 1.05$ redshift range, with bolometric luminosities ranging from 0.1 to 4×10^{44} erg s^{-1}.
7 clusters are found above a flux of 2×10^{-14} erg cm^{-2}s^{-1}. This translates to about 8.5/deg^2. We have investigated the L-T relation for the 9 clusters for which it was possible to measure a temperature. Results are displayed on Fig. 7 as a function of redshift. Malmquist bias is here obvious since a temperature was derived only for the apparently brightest clusters. The overall correlation appears the be quite tight and well summarizes the ability of rather shallow XMM survey-type observations to provide important new insights into the cluster population. This is particularly relevant for groups out to

[1]XMM exposure time is 20 ks over the region but we keep the same class definition as the S/N increase is only $\sqrt{2}$; the net effect being only a slight increase in C1/C2 number density ratio for this sub-region

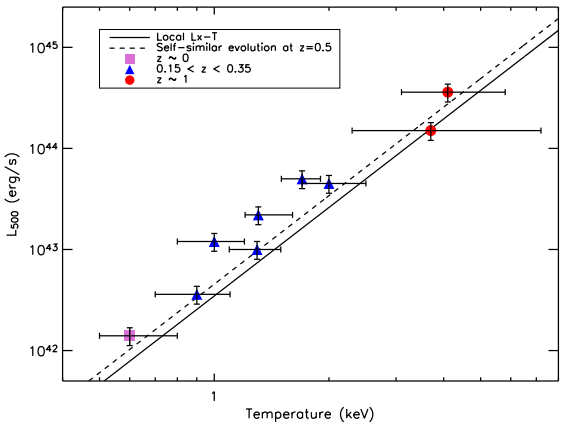

Figure 7. $L(R_{500})$-T relation for the D1 area clusters for which a temperature was obtained. The solid lines gives the mean local L-T relation, while the dotted line is the expected luminosity enhancement from the self-similar model, at a mean redshift of 0.5. The various symbols show the 3 distinct redshift (and luminosity/mass) regimes of the measured clusters.

$z \sim 0.4$ that the XMM-LSS is systematically unveiling for the first time. Our intermediate redshift subsample of groups (0.9-2 keV for $z_{med} = 0.25$) contains objects more luminous than predicted by the self similar evolution model. According to this hypothesis, the luminosity scales as the Hubble constant if it is integrated within a radius corresponding to a fixed ratio with respect to the critical density of the universe (Voit 2005). From the local universe, we know that low temperature groups show a larger dispersion in the L-T relation than massive clusters (Helsdon & Ponman 2003). This reflects their individual formation histories, since they are particularly affected by non-gravitational effects, as well as the possible contributions from their member galaxies. The apparent biasing toward more luminous objects and/or cooler system could come from the fact that we detect more easily objects having a central cusp, i.e. putative cool-core groups. This is under investigation using the full sample available from the current XMM-LSS area (Pacaud et al in preparation). Detailed presentation of the D1 catalogue and results are given by Pierre et al. (2005).

5. SUMMARY AND CONCLUSIONS

We have developed an X-ray pipeline enabling the construction, from shallow XMM pointings, of samples of galaxy clusters with controlled selection effects. In particular, "first class" clusters constitute a sample selected upon X-ray criteria alone (once nearby galaxies are removed). This approach offers the advantage of avoiding hypotheses about the faint end of the cluster LogN-LogS (currently not explored beyond the local universe) since this can become critical for faint samples said to be "flux limited". The C1 class contains objects as faint as $\sim 10^{-14}\ \mathrm{erg\,cm^{-2}s^{-1}}$ out to redshifts of unity. The final C1+C2 sample reaches a density of $12/\mathrm{deg}^2$ but the initial C2 selection has to be cleaned (by inspection of overlays and possibly optical spectroscopy) of a similar density of spurious cluster candidates ($\sim 5/\mathrm{deg}^2$).

We systematically unveil the low end ($T < 2$ keV) of the cluster population out to a redshift of 0.4. For the D1 CFHTLS area, we find a cluster density of 8.5 clusters per deg^2 having a flux larger than $2 \times 10^{-14}\ \mathrm{erg\,cm^{-2}s^{-1}}$. This is higher than the 4-5 clusters $/\mathrm{deg}^2$ given by the RDCS LogN-LogS (Rosati et al. 1998) and the shallow XMM/2dF survey (Gaga et al. 2005), which finds 7/2.3 = 3 $/\mathrm{deg}^2$ for the same flux limit. Given the size of the studied area, our results are certainly subject to cosmic variance which may also affect the 2.3 deg^2 XMM/2df survey and, to a lesser extent, the RDCS, which covers 5 deg^2 at $2 \times 10^{-14}\ \mathrm{erg\,cm^{-2}s^{-1}}$ (Rosati et al. 2002). For comparison, our simple cosmological model predicts some 7.5 clusters $/\mathrm{deg}^2$ having $T > 1$ keV above a flux of $2 \times 10^{-14}\ \mathrm{erg\,cm^{-2}s^{-1}}$ (Pacaud et al. 2005).

We present the first L-T relation from XMM survey-type observations over a contiguous area. The relation contains 9 clusters out to a redshift of unity over only $\sim 1\mathrm{deg}^2$ and so, opens remarkable perspectives for the study the evolution of the scaling laws for the cluster/group population with moderate XMM exposure times. On-going work aims at characterizing the evolution of the L-T relation for the $T < 2$ keV population over the currently available 7 deg^2 of the XMM-LSS (including the Subaru Deep Survey). In parallel, extensive simulations of XMM images enable us to investigate the effect of the cluster scaling laws (M-L-T-R), and of their evolution, on the survey selection function. These will be further constrained by the APEX and AMiBA Sunyaev-Zel'dovich surveys of the region to be performed in 2006. It will then be possible to model in a self-consistent way the cluster population in parallel with constraining cosmological parameters.

ACKNOWLEDGMENTS

This work is based on data obtained with XMM, VLT/FORS2, VLT/VIMOS, NTT/EMMI, Magellan/LDSS, and imaging campaigns performed at CTIO and CFHT[2].

REFERENCES

Arnaud, M. & Evrard, A. E. 1999, MNRAS, 305, 631

Arnaud, M., Pointecouteau, E., & Pratt, G. W. 2005, A&A, 441, 893

Bardeen, J. M., Bond, J. R., Kaiser, N., & Szalay, A. S. 1986, ApJ, 304, 15

Bennett, C. L., Halpern, M., Hinshaw, G., et al. 2003, ApJS, 148, 1

Bondi, M., Ciliegi, P., Zamorani, G., et al. 2003, A&A, 403, 857

Gaga, T., Plionis, M., Basilakos, S., Georgantopoulos, I., & Georgakakis, A. 2005, MNRAS, 870

Helsdon, S. F. & Ponman, T. J. 2003, MNRAS, 340, 485

Pacaud, F., Pierre, M., & et al. 2005, MNRAS, submitted

Pierre, M., Pacaud, F., & et al. 2005, MNRAS, submitted

Pierre, M., Valtchanov, I., Altieri, B., et al. 2004, Journal of Cosmology and Astro-Particle Physics, 9, 11

[2]The cluster optical images were obtained with MegaPrime/MegaCam, a joint project of CFHT and CEA/DAPNIA, at the Canada-France-Hawaii Telescope (CFHT) which is operated by the National Research Council (NRC) of Canada, the Institut National des Science de l'Univers of the Centre National de la Recherche Scientifique (CNRS) of France, and the University of Hawaii. This work is based in part on data products produced at TERAPIX and the Canadian Astronomy Data Centre as part of the Canada-France-Hawaii Telescope Legacy Survey, a collaborative project of NRC and CNRS

Rapetti, D., Allen, S. W., & Weller, J. 2005, MNRAS, 360, 555

Rosati, P., Borgani, S., & Norman, C. 2002, ARA&A, 40, 539

Rosati, P., della Ceca, R., Norman, C., & Giacconi, R. 1998, ApJ, 492, L21+

Sheth, R. K. & Tormen, G. 1999, MNRAS, 308, 119

Voit, M. 2005, Rev. Mod. Phys. (in press)

Willis, J. P., Pacaud, F., Valtchanov, I., et al. 2005, MNRAS, 363, 675